

Displacement damage cross section and mechanical properties calculation of an Es-Salam research reactor aluminum vessel

Djillali Saad¹ · Hocine Benkharfia² · Mahmoud Izerrouken³ · Ahmed Ali Benyahia⁴ · Hamid Ait-Abderrahim⁵

Received: 17 November 2016/Revised: 22 February 2017/Accepted: 2 March 2017/Published online: 26 October 2017
© Shanghai Institute of Applied Physics, Chinese Academy of Sciences, Chinese Nuclear Society, Science Press China and Springer Nature Singapore Pte Ltd. 2017

Abstract Nuclear facility aging is one of the biggest problems encountered in nuclear engineering. Radiation damage is among one of the aging causes. This kind of damage is an important factor of mechanical properties deterioration. The interest of this study is on the Es-Salam research reactor aluminum vessel aging due to neutron radiation. Monte Carlo (MC) simulations were performed by MCNP6 and SRIM codes to estimate the defects created by neutrons in the vessel. MC simulations by MCNP6 have been performed to determine the distribution of neutron fluence and primary knock-on atom (PKA) creation. Considering our boundary conditions of the calculations, the helium and hydrogen gas production in the model at a normalized total neutron flux of 6.62×10^{12} n/cm² s were determined to be 2.86×10^8 and 1.33×10^9 atoms/cm³ s, respectively. The SRIM code was used for the simulation of defects creation (vacancies, voids) in the aluminum alloy of the Es-Salam vessel (EsAl) by helium and hydrogen with an approximate energy of 11 MeV each.

The coupling between the two codes is based upon post-processing of the particle track (PTRAC) output file generated by the MCNP6. A small program based on the MatLab language is performed to condition the output file MCNP6 in the format of a SRIM input file. The concentration of silicon was determined for the vessel by the calculation of the total rate of $^{27}\text{Al}(n,\gamma)^{28}\text{Si}$ reaction. The DPA (displacement per atom) was calculated in SRIM according to R.E. Stoller recommendations; the calculated value is 0.02 at a fast neutron fluence 1.89×10^{19} n/cm². RCC-MRx standard for 6061-T6 aluminum was used for the simulation of the evolution of mechanical properties for high fluence. The calculated values of nuclear parameters and DPA obtained were in agreement with the experimental results from the Oak Ridge High Flux Isotope Reactor (HFIR) reported by Farrell and coworkers.

Keywords Radiation damage · EsAl · 6061-T6 · Silicon production · DPA · PKA · MCNP6 · SRIM · RCC-MRx · HFIR

✉ Djillali Saad
dsaad@usthb.dz

¹ Department of nuclear materials and mechanical test, Nuclear Research Center of Birine, BP 180, 17200 Ain-Oussera, Algeria

² Reactor Physics Department, Nuclear Research Center of Birine, BP 180, 17200 Ain-Oussera, Algeria

³ Reactor Physics Department, Nuclear Research Center of Draria, BP 43 Sebala, 16050 Draria, Algeria

⁴ Advanced Mechanics Laboratory, University of Sciences and Technology Houari Boumediene, BP 32 El Alia, 16111 Bab Ezzouar, Algeria

⁵ SCK-CEN, Belgian Nuclear Research Centre, Boeretang 200, 2400 Mol, Belgium

1 Introduction

Aluminum alloys (5000 and 6000 series) are well used in nuclear technology as fuel cladding, structural materials, and reactor tanks [1, 2]. During the reactor operation, these alloys experience radiation damage resulting in continuous aging and limitation of its life span. Consequently, aging management of the material principally reactor vessel, which is difficult to replace, is important [3]. For this purpose, establishment of a material properties database is needed to estimate the safety lifetime of the structural materials used in nuclear reactors. For our knowledge,

there are not enough published papers about the irradiation behavior of aluminum alloys under the operation conditions of research reactors. Therefore, in the present investigation, we developed a method based on MCNP6 [4] and SRIM [5] codes to calculate the displacements damage caused by N_{dpa} in the Es-Salam research reactor aluminum vessel. We used also RCC-MRx standards for 6061-T6 aluminum to simulate the evolution of its mechanical properties. Our aim is to predict the Es-Salam reactor vessel lifetime under the irradiation environments and operation condition of such a reactor.

2 Radiation displacement damage

Radiation damage induced in the aluminum structural materials depends on the composition, manufacturing circumstances, irradiation temperature, neutron spectrum, thermal, and fast neutron. In the thermal neutron field, aluminum atoms are transmuted to silicon according to the $^{27}\text{Al}(n,\gamma)^{28}\text{Si}$ reaction. The silicon precipitates grow with increasing fluence. In the case of aluminum alloys of the 5000 series, the main alloying element, Mg, is in solution. The production of silicon under irradiation causes a precipitation of Mg_2Si , which induces an increase of mechanical strength and a loss of ductility [6]. However, in structural alloys of the 6000 series, the main alloying elements Mg and Si are fine precipitates obtained by heat treatment, therefore only the Mg content in excess of the stoichiometric composition Mg_2Si is available for further precipitation with silicon produced by irradiation [6].

Moreover, the solvability of Al for Si is very low so in the case of the absence of an additional alloy like Mg, silicon is precipitated by crystallization at the grain boundaries. It is seen in earlier findings that Si precipitates with a diameter of 170 Å, and a concentration of $10^{16}/\text{cm}^3$ was observed in Al6061 irradiated to thermal and fast neutron fluence of $9.2 \times 10^{22} \text{ n/cm}^2$ and of $11.6 \times 10^{22} \text{ n/cm}^2$, respectively [7]. The Si precipitates accumulation induces swelling and increases tensile strength and reduction of ductility [7, 8]. We note that the transmutation reaction due to the thermal neutron capture is the major part of the defect source in the case of thermal to fast neutron ratio higher than 400 [9]. In the later case, the Si precipitates are responsible for most of the radiation strengthening in 6061-T6 alloys.

Fast neutrons ($E > 1 \text{ MeV}$) induce displacement via elastic scattering with target atoms and nuclear reactions, principally $^{27}\text{Al}(n,\alpha)^{24}\text{Na}$ and $^{27}\text{Al}(n,p)^{27}\text{Mg}$ with neutron energy threshold of 6 and 1.9 MeV, respectively. According to Kelly [10], approximately 300 displacements are caused in average by fast neutrons ($E > 1 \text{ MeV}$) resulting in a change of mechanical properties. Both recoil atoms,

called primary knock atom, and nuclear reaction products, alpha particles (α) and proton (p), impart energy to neighboring atoms and produce large displacement cascades along their path. This is possible if the PKA energy is higher than the threshold displacement energy, E_d . For collisions in which the lattice atom receives energy less than E_d , the struck atom undergoes large amplitude vibrations within its potential well but remains in its lattice site. Once initiated by the PKA atom, collisions continue occurring until energy in excess of E_d is dissipated, typically after about 10 ps. An illustration of a typical PKA event in a simple lattice is shown in Fig. 1 [11]. Various models were proposed to calculate the number of displaced atoms produced by the recoil atom of energy E . The most widely cited model was that of Kinchin and Pease [12]. Their model assumed that between threshold energy and energy cutoff, there is a linear relationship between the number of Frenkel pair produced and the PKA energy. Below the threshold displacement energy, no new displacements would be produced. Above the high-energy cutoff, it is assumed that the additional energy is dissipated in electronic excitation and ionization. Lindhard and coworkers [13] developed a detailed theory for energy partitioning that could be used to compute the fraction of the PKA energy that was dissipated in the nuclear system in elastic collisions and in electronic losses. This work was used by Norgett, Robinson, and Torrens (NRT) to develop a secondary displacement model that is still used as a standard in the nuclear industry and elsewhere to compute atomic displacement rates [14]. The NRT model is governed by the following equation:

$$N_d(T_d) = \begin{cases} 0 & T_d < E_d \\ 1 & E_d \leq T_d < 2E_d/\beta \\ \beta T_d/2E_d & 2E_d/\beta \leq T_d \leq \infty \end{cases} \quad (1)$$

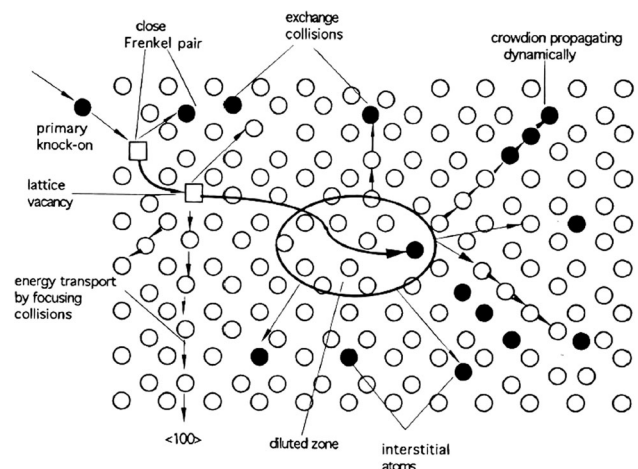


Fig. 1 Atomic displacement processes in energetic displacement cascade envisioned by A. Seeger in 1958

where $N_d(T_d)$ is the number of displaced atoms produced by recoil atom of energy, E , and damage energy T_d and E_d is the average threshold displacement energy [15]. β (equal to 0.8) is known as the scattering correction factor. The damage energy (T_d) in the above expression is a function of E_{PKA} . The damage energy is the amount of the initial PKA energy available to cause atomic displacements, with the fraction of the PKA's initial kinetic energy lost to electronic excitation being responsible for the difference between E_{PKA} and T_d . It is calculated for each recoil energy using Robinson's analytic expression [16]. The threshold displacement energy, E_d , is dependent on the material structure and can be determined experimentally or by molecular dynamics simulation. In the present study, a value of 25 eV is used [15]. The displacement defects consist of point defects (vacancies and interstitial). With increasing fast neutron fluence, the vacancy clusters are developed to voids and dislocations. Mean void diameter of 370 Å and concentration of about $1.9 \times 10^{14}/\text{cm}^3$ were measured in Al6061 and irradiated to thermal and fast neutron fluence of $9.2 \times 10^{22} \text{ n cm}^{-2}$ and of $11.6 \times 10^{22} \text{ n/cm}^2$, respectively, by King et al. [7]. According to these authors, the voids generate a swelling of 0.68% at this fluence.

3 Material and calculation method

Aluminum alloy of Es-Salam reactor vessel (EsAl) is part of the 6000 series (Al–Mg–Si) and is very close to the 6061 shades which are widely used in the manufacture of sensitive structure research reactors. However, its chemical composition is a little bit different from the latter in terms of ratio of the main components (Mg and Si) that are nearly inverted in the two aluminums [17]. The chemical composition of the aluminum vessel of the Es-Salam research reactor is given in Table 1.

3.1 Displacement damage calculation

The simulation of reactor neutron induced damage in structural materials is well investigated using different methods. Jonghwa et al. [18], have investigated radiation damage in SiC using the combination of NJOY and SRIM codes. Heinish et al. [19] used SPECOMP and SRIM codes to calculate the damage cross section in SIC irradiated in

the fission reactor. Neutron induced damage under a variety of neutron energy spectra was also investigated by several authors using a combination of MCNP and SRIM codes [20–22].

The generalized MC transport code, MCNP, was used to model the interaction of neutrons with material [23]. It is specifically designed for computing accurate neutron physics, the tracking of particles through specified problem geometry [24]. It utilizes continuous energy nuclear cross section libraries to evaluate the likelihood of interaction at each point. MCNP6 can easily tabulate additional parameters which would be useful in a more rigorous multi-scale model of radiation damage. Such parameters include nuclear heating, internal gas production (He, H, etc.), and photon production as well as many reaction rates of interest. The MCNP6 tally that is of event-by-event nature and fit the study requirement is the PTRAC card.

The SRIM software, previously known as TRIM, has gained wide popularity in the ion irradiation community. The primary reasons are that, on the one hand it is free and easy to install and use in a Windows operating system, on the other hand it can calculate ion penetration depth profiles for any kind of ion with energies from a few tens of eV to 1 GeV in any material.

The SRIM software treats the ion penetration in a material with the binary collision approximation, i.e., as a series of independent binary collisions. The SRIM calculations can be run in two different modes: “Ion distribution and quick calculation of damage” and “Detailed calculation with full damage cascades.” In the former, only the path of the incoming ion is followed. In the latter, also all knock-on atoms of all generations (primary, secondary, etc.) that have an energy above the threshold energy are followed. Stoller et al. [25], recommended an interesting recipe for obtaining DPA values for metals using SRIM code.

The coupling between the two codes (MCNP6 and SRIM) is made using a home program based on the MatLab language in order to adjust the output file of MCNP6 to the input file of SRIM.

MCNP6 transport programs are used to calculate where neutron collisions are made in the target, and give the position, and recoil statistics for each collision atom. Then, SRIM calculates the full target recoil cascade. A file called TRIM.DAT was generated and gives radiation damage events.

Table 1 Characteristics of the vessel material [17]

Material	Density (g/cm ³)	Al (%)	Mg	Si	Fe	Cu	Ti	Zn	Cr
EsAl	2.7	≥ 98.13	0.45–0.9	0.6–1.2	≥ 0.2	≤ 0.01	≤ 0.01	≤ 0.03	≤ 0.03

Table 2 factors $f_{p0.2}^{ir}$ and f_m^{ir} at $T = 50\text{ }^\circ\text{C}$

Φ_{th} (10^{21} n _{th} /cm ²)	$f_{p0.2}^{ir}$	Φ_{th} (10^{21} n _{th} /cm ²)	f_m^{ir}
$\Phi_{th} \leq 1.2$	1	$\Phi_{th} \leq 1.8$	1
$1.2 < \Phi_{th} \leq 300$	$-4.3928 + 0.1111 \text{Ln}(\Phi_{th})$	$1.8 < \Phi_{th} \leq 300$	$-3.6151 + 0.0943 \text{Ln}(\Phi_{th})$

Table 3 A_{gt} and A_t after irradiation

Φ_{th} (10^{21} n _{th} /cm ²)	A_{gt} (%)	Φ_{th} (10^{21} n _{th} /cm ²)	A_t (%)
$5.5 < \Phi_{th} \leq 476$	$248.441 - 10.397 \text{Log}(\Phi_{th})$	$34 < \Phi_{th} \leq 532$	$-3.6151 + 0.0943 \text{Ln}(\Phi_{th})$
$\Phi_{th} > 476$	2.24	$\Phi_{th} > 532$	2.5

3.2 Mechanical properties calculation

To simulate the mechanical properties after irradiation, we followed the methodology of the RCC-MRx standard [26]. The principle of this methodology is:

To obtain the yield strength after irradiation of a material, simply multiply the value of the yield strength before irradiation by a factor that supports the material behavior after irradiation. While our material EsAl is shaded very close to that of 6061-T6, we used the same factors after irradiation that are given by the RCC-MRx standard. The average yield strength at 0.2% offset $R_{p0.2}^{after}$ is obtained by multiplying the average yield strength at 0.2% offset $R_{p0.2}^{before}$ before irradiation by the factor $f_{p0.2}^{ir}$. The average tensile strengths, R_m^{after} , are obtained by multiplying the average tensile strength, R_m^{before} , before irradiation by the factor f_m^{ir} . The factors $f_{p0.2}^{ir}$ and f_m^{ir} are given as a function of the fluence, Φ_{th} , by the formulae in Table 2.

The ductility characteristics are percentage total elongation at fracture A_t and percentage total elongation at maximum force A_{gt} . To simulate the evolution of elongation after irradiation according to RCC-MRx standard, the decrease of elongation fulfills a function of the form:

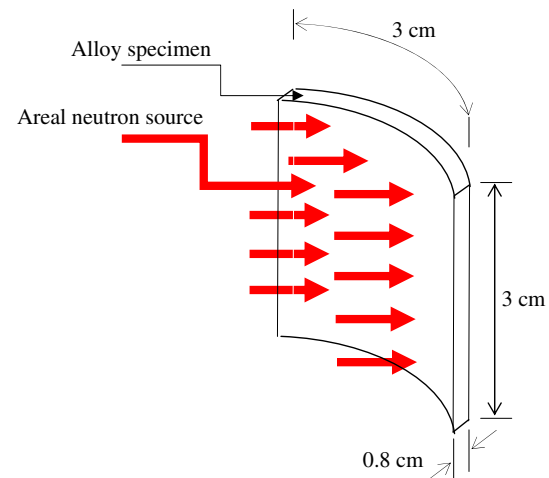
$$\text{Elongation (\%)} = A - B \text{Log}(\Phi_{th}). \quad (2)$$

Based on the A_{gt} and A_t values before irradiation, the constants A and B are determined for each fluence range. A_{gt} and A_t are given as a function of the fluence Φ_{th} by the formulae in Table 3.

4 Results

4.1 DPA Calculation

A model of the Es-Salam reactor core, as well as KCODE calculation and F4 tallies, was built on the MCNP6 platform to calculate the average neutron spectrum on the wall of the vessel for three energy groups of thermal, epithermal, and fast neutrons (from zero to twenty

**Fig. 2** (Color online): EsAl alloy model for 3D-MCNP6 calculation

MeV). This spectrum is subsequently applied on a model of the vessel $3\text{ cm} \times 3\text{ cm} \times 0.8\text{ cm}$ slab (Fig. 2). FMn cards have been used in the input file of MCNP6 to generate (n, γ) , (n, p) , and (n, α) neutron reactions.

The average total unnormalized neutron flux in the specimen is 3.7075×10^{-5} n/cm² s, and normalized neutron flux is 6.62×10^{12} n/cm² s. The average normalized thermal flux is 6.09×10^{12} n/cm² s ($E \leq 0.55$ eV), the epithermal flux is 1.88×10^{11} n/cm² s ($0.55\text{ eV} < E \leq 0.1\text{ MeV}$), and the fast flux is 3.42×10^{11} n/cm² s ($E \geq 2\text{ MeV}$). The total unnormalized number of PKA is 9.0732×10^{-9} atoms/cm³ s and normalized number of PKA is 1.616×10^9 atoms/cm³ s, which has been determined by the number of scatters on the EsAl aluminum atoms in a neutron energy range from 0.1 to 20 MeV. The minimum neutron energy necessary to displace the atom from the crystal lattice (PKA) is 100 keV and the threshold energy displacement (E_d) is 25 eV. The total particle production in the specimen is given in Table 4.

Figure 3 shows the PKA energy thresholds (α and p) through the thickness of the vessel. Considering the damage energy as the sum of the damage energy to target atoms and phonons [25], it is found from the calculation that the total number of DPA generated by the proton and He in

Table 4 Nuclear reaction in the material

Target atom	Reaction and product	Unnormalized production in model (Atom/cm ³ s)
²⁷ Al	²⁷ Al(n,α) ²⁴ Na	1.60172 × 10 ⁻⁹
	²⁷ Al(n,p) ²⁷ Mg	7.47150 × 10 ⁻⁹
	²⁷ Al(n,γ) ²⁸ Si	6.71028 × 10 ⁻⁶

EsAl as a function of fast neutron fluence (Φ_f) can be represented by the following equation:

$$DPA_{SRIM} = 1.029 \cdot 10^{-21} \Phi_f \tag{3}$$

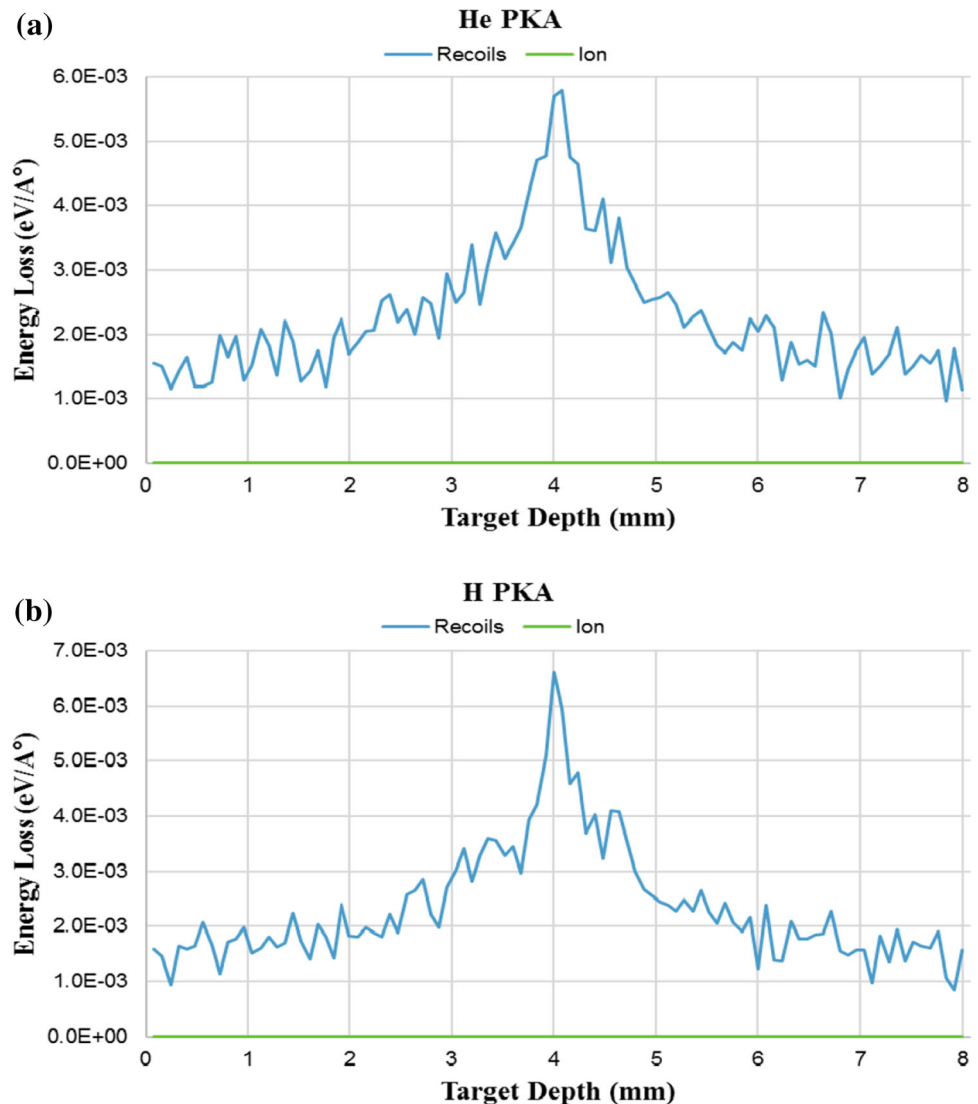
MCNP6 was also used to calculate the DPA within the aluminum vessel. The DPA was calculated using the ENDF-B-VI damage cross sections (Fig. 4), which are not a part of the MCNP6 default cross section libraries. The ENDF-B-VI cross sections were developed using the NRT

model and combined BCA-MD method [27]. The DPA was calculated in MCNP6 according to the equation:

$$DPA_{XC} = \frac{\int dv \int \varphi(\vec{r}, E) dE \sum_{i=1}^N X_i \sigma_i^{dpa}(E)}{\sum_{i=1}^N 2E_{d,i}} \tag{4}$$

where $\sigma_i^{dpa}(E)$ is the displacement cross section, $\varphi(\vec{r}, E)$ is the neutron flux and dv is the considered volume. The MT number of damage cross section is 444. This number is used in the FM card in MCNP6. Using this tally, MCNP6

Fig. 3 (Color online): PKA loss energy in the target atom. **a** He PKA loss energy, **b** H PKA loss energy



calculated the rate of displacements per atom of 3.18×10^{-10} DPA s^{-1} . The DPA can be represented as a function of fast fluence by the following equation:

$$DPA_{XC} = 0.929 \cdot 10^{-21} \Phi_f \tag{5}$$

This result agrees well with the results already found with the coupling of the codes MCNP6 and SRIM.

Figure 5 shows the DPA evolution as a function of fast neutron fluence in the Es-Salam reactor vessel (EsAl) compared to the experimental data of Al6061-T6 irradiated at HFIR [23]. As can be seen, Eqs. (3) and (5) simulate very well the experimental DPA values (Fig. 5).

4.2 Silicon production

The concentration of silicon was determined for the EsAl vessel by the calculation of the total rate of $^{27}\text{Al}(n,\gamma)^{28}\text{Si}$ reaction. The unnormalized reaction rate of $^{27}\text{Al}(n,\gamma)^{28}\text{Si}$ from thermal and epithermal neutrons is

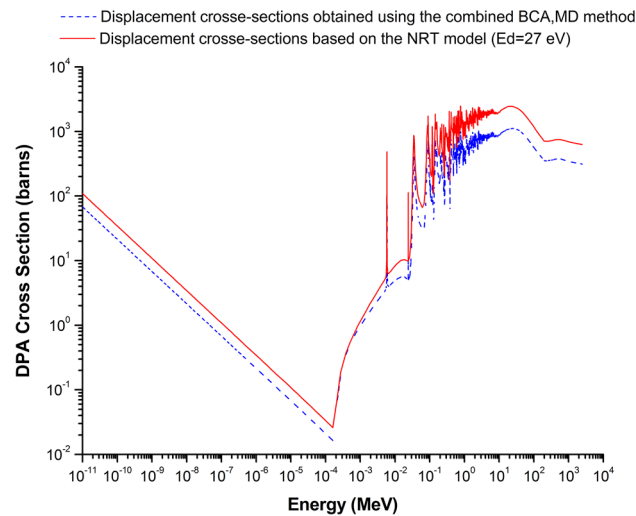


Fig. 4 ^{27}Al ENDF/B-VI DPA cross sections [27]

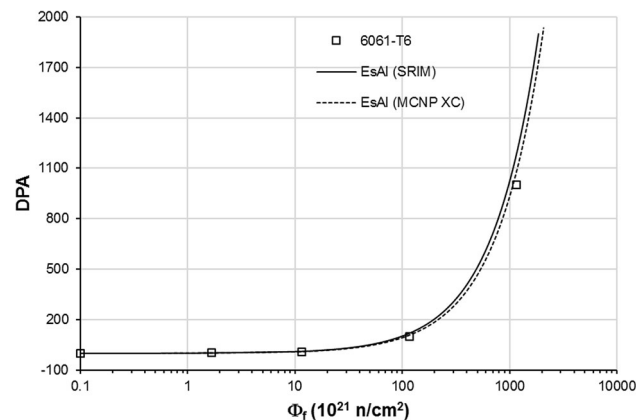


Fig. 5 MCNP6-SRIM calculated DPA and HFIR DATA

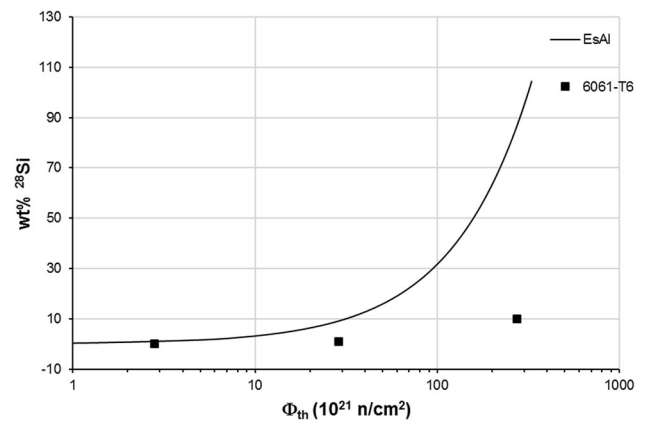


Fig. 6 Thermal fluence dependence of created silicon content in EsAl alloy

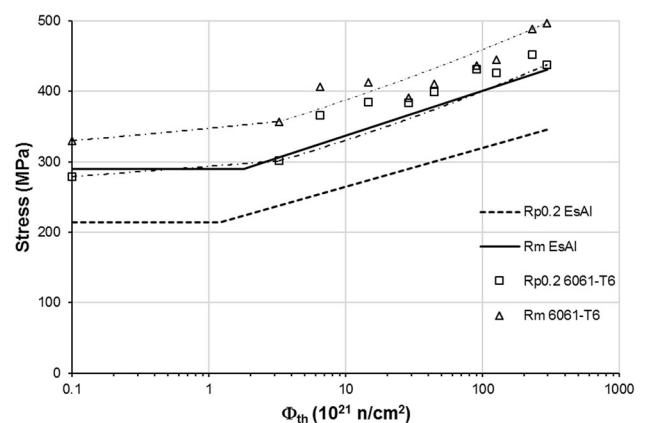


Fig. 7 Fluence dependence of $R_{p0.2}$ and R_m of EsAl and Al6061-T6 compared with data of 6061-T6 irradiated at HFIR

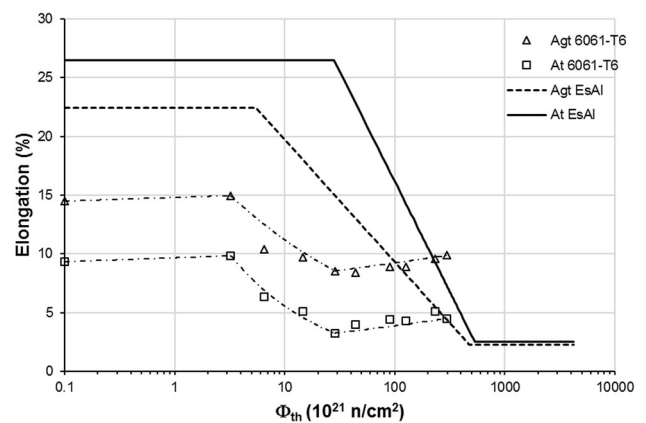


Fig. 8 Fluence dependence of A_{gt} and A_t of EsAl compared with HFIR of 6061-T6

about 6.83×10^{-6} atoms/ cm^3 s. Taking into account the volume calculation and the atomic density of the studied material, we find a linear relationship between the created silicon content and the thermal fluence (Eq. 6). The amount

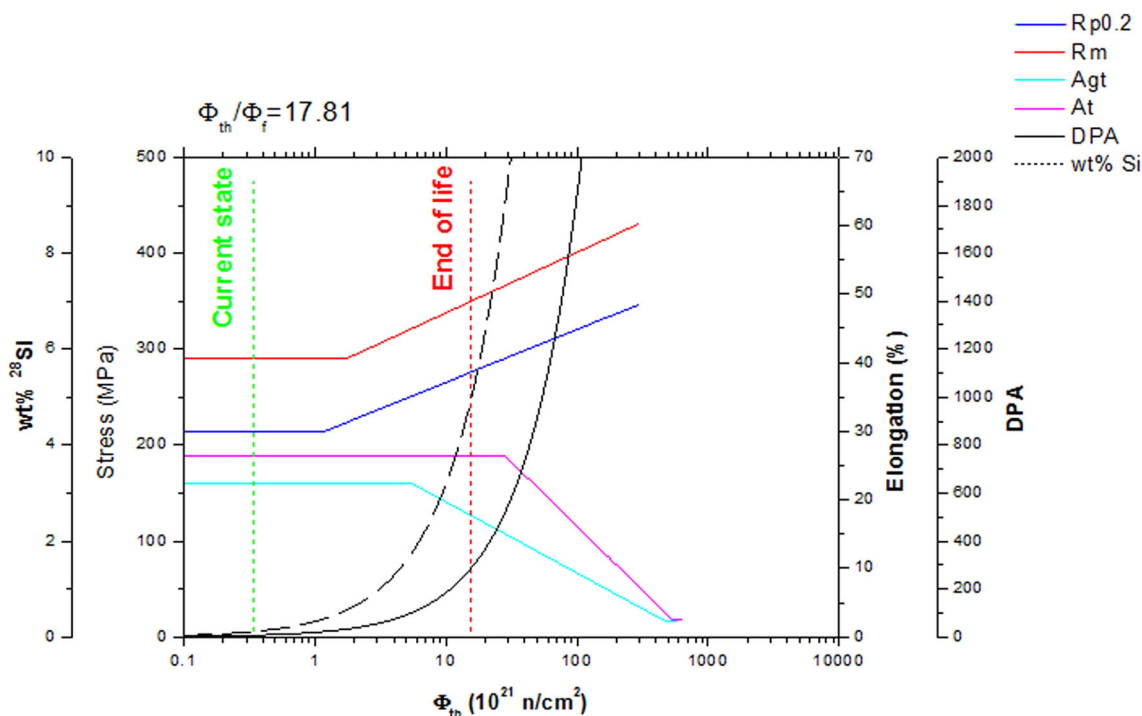


Fig. 9 Fluence dependence of mechanical properties of the vessel research reactor Es-Salam

of silicon produced in the Es-Salam reactor vessel using this equation is presented in Fig. 6 and compared to the Si concentration formed in Al6061-T6 irradiated at HFIR reactor [28]. It is clear from the figure that a good concordance is found between simulation and experimental data in the fluence range lower than $3 \times 10^{22} \text{ n/cm}^2$.

$$\text{wt} \% \text{ } ^{28}\text{Si} = 3.18 \cdot 10^{-22} \Phi_{th}. \tag{6}$$

The difference in the results for the height fluences is due to the two distinct ratios (thermal flux to fast flux). Indeed, the HFIR samples were irradiated with a ratio equal to 1.66 whereas the sample of our study was simulated with a ratio of 17.81. Let us note here that most neutrons arriving at the level of the vessel are moderate. The HFIR samples were taken from the control bar tubes which is why the ratio of thermal flux to the fast flux in the case of HFIR is much less than those of the Es-Salam reactor.

Weeks et al. [29] study indicates that the increase in tensile strength and decrease in ductility result primarily from the thermal fluence, i.e., the transmutation of aluminum to silicon. In regions where the thermal flux is greater than the fast flux, more rapid mechanical properties degradation can be expected than in areas where fast flux is dominant.

4.3 Mechanical properties simulation

The simulation of the mechanical properties was made using the methodology of the RCC-MRx standard [26] described above.

Figure 7 shows the fluence dependence of $R_{p0.2}$ and R_m of EsAl and Al6061-T6 compared with the data of 6061-T6 irradiated at HFIR [28]. The chemical composition of the 6061 alloy was 0.87 wt% Mg and 0.58 Si. Button-headed tensile specimens of gage length 28.6 mm and gage diameter 3.2 mm were machined from cold-swaged bars and were heat-treated as T6 temper. The specimens were irradiated in the peripheral target positions in HFIR in contact with the cooling water at about 55 °C for periods up to 3.5 years during which they accumulated fast neutron fluences up to $1.8 \times 10^{23} \text{ n/cm}^2$ and thermal fluences up to $3.0 \times 10^{23} \text{ n/cm}^2$.

As can be seen, the calculated $R_{p0.2}$ and R_m for Al6061-T6 are approximately similar to the experimental data. However, the calculated $R_{p0.2}$ and R_m values of EsAl are lower than that 6061-T6 indicating probably the higher radiation resistance of EsAl.

4.4 Ductility characteristics

Figure 8 shows the fluence dependence of A_t and A_{gt} of EsAl and Al6061-T6 compared with the data of 6061-T6 irradiated at HFIR. It is clear from the figure that the

calculated A_t and A_{gt} for Al6061-T6 reproduce the experimental data. However, the calculated A_t and A_{gt} values of EsAl are higher than that 6061-T6. The calculated values of ductility show an advantage in favor of the ESAI material.

4.5 Vessel lifetime Estimation

Actually, the existing thermal and fast ($E > 0.1$ MeV) neutron fluence at the Es-Salam research reactor vessel are, respectively, 3.37×10^{20} n/cm² and 1.89×10^{19} n/cm². According to our calculation, at such fluence, the obtained displacement density is 0.02 dpa, and only 1.23 ppm hydrogen atoms and 0.26 ppm helium are produced in the aluminum structure. The amount of silicon produced is 0.107%wt. Figure 9 resumes the mechanical properties evolution of the Es-Salam research reactor vessel as a function of fluence. The green vertical line represents the current state. As can be seen, the critical value for the elongation representing the end-of-life-value (red line) is reached at a neutron fluence of 1.57×10^{22} n/cm² which corresponds to 5%wt ²⁸Si and about 1100 dpa. The wt% ²⁸Si product in the Es-Salam aluminum vessel is considerably lower than the end-of-life limit. Based on the mode of operation of 60 MW days per year [30], the power operation of the reactor could be continued for additional 1.607×10^6 MWh.

5 Conclusion

The simulations of radiation damage in Es-Salam research reactor were carried out using the MC transport code MCNP6 and the Transport Range of Ions in Matter code SRIM. The calculations have been performed using the continuous energy MCNP6 transport code to determine the nuclear parameters in the Es-Salam research reactor vessel. The parameters include high-energy neutron fluence distribution, the defect production in form of primary knock-out atoms, and H and He atoms. On the basis of MCNP6 modeling of radiation damage in the aluminum structure of the vessel of the Es-Salam research reactor, following conclusions are made:

- Under consideration of the total power history of the Es-Salam research reactor, the dpa number and silicon produced are too low to cause any increase in the tensile strength and reduction of ductility.
- The change of the mechanical properties of aluminum due to the fast neutron damage is considerably low for any consequences.

However, good agreement was found between our calculated values and the experimental data. Thus, we

conclude that the developed model is capable of accurately determining radiation damage in any structure and location of the reactor core.

Acknowledgements We thank Dr. T. ZIDI for the execution of the MCNP6 code. We are most grateful to Prof. H. Ait-Abderrahim for the valuable assistance related to the use of RCC-MRx standard. Many thanks to Dr. S. Hadji for very interesting information related to the interpretation of units used by SRIM code.

References

1. F. Ozturk, A. Sisman, S. Toros et al., Influence of aging treatment on mechanical properties of 6061 aluminum alloy. *Mater. Des.* **31**, 972–975 (2010). doi:10.1016/j.matdes.2009.08.017
2. M. Kolluri, Radiation Effects in Materials, in *Neutron Irradiation Effects in 5xxx and 6xxx Series Aluminum Alloys: A Literature Review*, ed. by A. Waldemar (Intech, Monteiro, 2016), pp. 393–411
3. H. Ju Jin, T. Kyu Kim, Neutron irradiation performance of Zircaloy-4 under research reactor operating conditions. *Ann. Nucl. Energy* **75**, 309–315 (2015). doi:10.1016/j.anucene.2014.08.042
4. M. R. James, D. B. Pelowitz et al., Technical Report: MCNP6 User's Manual Code Version 6.1.1beta (LA-CP-14-00745, 2011), (Los Alamos National Laboratory, 2014)
5. SRIM-2013 software package (2013), <http://www.srim.org/SRIM/SRIMLEGL.htm>. Accessed Sept 2014
6. B. Kapusta, C. Sainte-Catherine, X. Averty et al., Present status on the mechanical characterization of aluminum alloys 5754-NET-O and 6061-T6 irradiated at high fluences. Paper presented at the 9th Meeting of the International Group on Research Reactors, IGORR, Sydney, Australia, 24–28 March 2003
7. R. T. King, A. Jostsons, K. Farrell, in the Seventy-fifth Annual Meeting: Topics in the Effect of radiation on substructure and mechanical properties of metals and alloys, ed. by ASTM. A symposium presented at the Seventy-fifth Annual Meeting, Los Angeles, Calif., 25–30 June 1972. Neutron Irradiation Damage in a Precipitation-Hardened Aluminum Alloy, ASTM STP 529 (ASTM, Los Angeles, 1973), pp. 165–180
8. N.R. Mc Donald, C.J. Moss, The Ageing of the HIFAR Aluminum Tank: A Case Study. Paper presented at in IAEA Seminar for Asia and the Pacific on Ageing of Research Reactors, (Bangkok, Thailand, 1992)
9. K. Farrell, Report: Assessment of aluminum structural materials for service with the ANS reflector vessel (ORNL/TM-13049), IAEA, August 1995
10. B.T. Kelly, *Irradiation damage to solids*, 1st edn. (Pergamon Press, Oxford, 1966), p. 180
11. R.S. Averback, T. Diaz De La Rubia, Displacement Damage in Irradiated Metals and Semiconductors, in *Solid State Physics*, vol. 51, ed. by H. Ehrenreich, F. Spaepen (Academic Press, Cambridge, 1998), pp. 281–402
12. G.H. Kinchin, R.S. Pease, The mechanism of the irradiation disordering of alloys. *J. Nucl. Energy I*, 200–202 (1955). doi:10.1016/0891-3919(54)90016-9
13. J. Lindhard, M. Scharff, H.E. Shiott, *Report: Range concepts and heavy ion ranges (Notes on Atomic Collisions II)* (Academy of Sciences, Royal Danish, 1963)
14. M.J. Norgett, M.T. Robinson, I.M. Torrens, A proposed method of calculating displacement dose rates. *Nucl. Eng. Des.* **33**, 50–54 (1975). doi:10.1016/0029-5493(75)90035-7

15. ASTM E521-16, Standard Practice for Investigating the Effects of Neutron Radiation Damage Using Charged-Particle Irradiation, ASTM International. (West Conshohocken, PA, 2016)
16. M. T. Robinson, in Proceedings of Nuclear Fusion Reactors, London, 1970, ed. by British Nuclear Energy Soc. (UKAEA)
17. R. SHA, B. ZHU, J. LIU et al., Report: Study on corrosion of LT-21 aluminum alloy samples hung in reactor (China Nuclear Information Centre), (Atomic Energy Press, 1998)
18. J. Chang, J.Y. Cho, C.S. Gil et al., A simple method to calculate the displacement damage cross section of silicon carbide. *Nucl. Eng. Technol.* **46**, 475–480 (2014). doi:[10.5516/NET.01.2013.051](https://doi.org/10.5516/NET.01.2013.051)
19. H.L. Heinisch, L.R. Greenwood, W.J. Weber et al., Displacement damage cross sections for neutron-irradiated silicon carbide. *J. Nucl. Mater.* **327**, 175–181 (2004). doi:[10.1016/s0022-3115\(02\)00962-5](https://doi.org/10.1016/s0022-3115(02)00962-5)
20. P. Domonkoš, G. Farkas, Computer Simulation by MCNP-4C2 and TRIM 98.01 Codes. Paper presented at the Anniversary of Nuclear Technology 2004, Duesseldorf, Germany, 2004
21. G. Farkas, P. Domonkoš, V. Slugeň et al., Nuclear Analysis of the Copper Alloys for Fusion Technologies by Monte Carlo Method. *Comput. Mater. Sci.* **36**, 121–124 (2006). doi:[10.1016/j.comatsci.2004.11.021](https://doi.org/10.1016/j.comatsci.2004.11.021)
22. S. Bofo, Thesis: Simulation of defects in (Be, Al) by neutron irradiation in the Ghana Research Reactor (GHARR-1) core using the MCNP5 and TRIM codes, (University of Ghana, 2012)
23. M. Tajik, N. Ghal-Eh, G.R. Etaati et al., Modeling NE213 scintillator response to neutrons using an MCNPX-PHOTRACK hybrid code. *Nucl. Instrum. Methods Phys. Res. Sect. A* **704**, 104–110 (2013). doi:[10.1016/j.nima.2012.12.001](https://doi.org/10.1016/j.nima.2012.12.001)
24. L. Hamidatou, H. Benkharfia, Experimental and MCNP calculations of neutron flux parameters in irradiation channel at Es-Salam reactor. *J. Radioanal. Nucl. Chem.* **287**, 971–975 (2011). doi:[10.1007/s10967-010-0922-9](https://doi.org/10.1007/s10967-010-0922-9)
25. R.E. Stoller, Primary Damage Radiation Formation. Oak Ridge Natl. Lab. (2012). doi:[10.1016/B978-0-08-056033-5.00027-6](https://doi.org/10.1016/B978-0-08-056033-5.00027-6)
26. AFCEN, Design and Construction Rules for Mechanical Components of Nuclear Installations (RCC-MRx 2012). (AFCEN, France, 2012)
27. DXS displacement damage cross-section data file (Karlsruhe Institute of Technology, October 2010), <https://www-nds.iaea.org/CRPdpa/>. Accessed Jan 2017
28. K. Farrell, R.T. King, Tensile properties of neutron-irradiated 6061 aluminum alloy in annealed and precipitation-hardened conditions. *ASTM STP* **683**, 440–449 (1979)
29. J. R. Weeks, C. J. Czajkowski, P. R. Tichler, in 14th International Symposium: Topics in Effects of Radiation on Materials, ed. by N. H. Packan, R. E. Stoller and A. S. Kumar. 14th International Symposium on Effects of Radiation on Materials, Philadelphia, 1990. Effects of High Thermal and High Fast Fluences on the Mechanical Properties of Type 6061 Aluminum in the HFBR, vol. II (ASTM, Philadelphia, 1990), pp. 441–452
30. Es-Salam DZ0002 (IAEA, 2009), <https://nucleus.iaea.org/RRDB/RR/Utilization.aspx?RId=115>, Accessed 05 Sept 2016